Microscopic investigation of the $\alpha + {}^{18}O$ system in a three-cluster model

P. Descouvemont
Physique Théorique et Mathématique, Université Libre de Bruxelles, Brussels, Belgium
(Received 16 February 1988)

The ^{22}Ne spectrum is investigated with microscopic wave functions defined in the generator-coordinate formalism. This nucleus is described in a three-cluster model, involving an ^{16}O core surrounded by a dineutron and an α particle. The ^{18}O cluster is projected out on the 0^+ and 2^+ states. We propose a band structure of ^{22}Ne with experimental candidates. The model suggests the existence of a 0^+ band presenting a marked $\alpha + {}^{18}O$ cluster structure. We present the $\alpha + {}^{18}O(0^+, 2^+)$ collision matrices, and discuss the resonance properties in the $^{18}O(\alpha,\alpha)^{18}O$ scattering. Electromagnetic transition probabilities in the ^{22}Ne nucleus are calculated. From the theoretical Coulomb shifts between the mirror ^{22}Ne and ^{22}Mg nuclei, we suggest spin assignments for different ^{22}Mg states. The $^{18}O(\alpha,\gamma)^{22}Ne$ capture cross section is calculated, and is used for determining microscopically the nonresonant reaction rate.

I. INTRODUCTION

Microscopic calculations provide information on the properties of the collision between two composite particles, and on the spectroscopy of the unified nucleus. They represent a basic approach since, except in the nucleon-nucleon interaction, they do not contain any free parameter. Furthermore, microscopic theories give a unified description of bound, resonant, and scattering states of a dinuclear system. This property is especially useful in radiative capture calculations, for example, which involve bound and scattering states simultaneously. The generator-coordinate method[1] (GCM) has been shown to represent a powerful method for the microscopic investigation of many systems. Recently, we have applied the GCM to several reactions and to the study of light nuclei (see, e.g., Ref. 2 and references therein). The α clustering is well known in many nuclei.[3] A large number of microscopic investigations have been devoted to its study. However, these approaches are usually restricted to nuclei involving an α particle and a nucleus whose description in the harmonic-oscillator model is rather easy. Recently, we have applied a microscopic three-cluster model which allows us to go beyond the usual one-center description of the nuclei involved in the reaction. We have shown in the three-cluster study of the $\alpha + {}^{8}Be$ system,[4] that the clustering in ^{8}Be has to be taken into account for reproducing reasonably the ^{12}C properties. We have extended the three-cluster model to the $\alpha + {}^{20}Ne$ study,[5] where the ^{20}Ne nucleus is described in the $\alpha + {}^{16}O$ cluster structure. In this paper we aim at investigating the $\alpha + {}^{18}O$ structure of ^{22}Ne in the same framework. The ^{18}O nucleus can be described, for the lowest states, by an ^{16}O core surrounded by a two-neutron cluster (dineutron). Owing to the flexibility of the model, we may include the $\alpha + {}^{18}O(0^+, 2^+)$ channels simultaneously. It is well known[6] that the inclusion of excited configurations enlarges the variational basis, and improves the wave functions. Moreover, it leads to a number of ^{22}Ne states larger than in a single-channel approach. The $\alpha + {}^{18}O$ system has already been studied by Langanke *et al.* in single-channel[7] and multichannel[8] calculations, with a filled *p* shell, and two neutrons in the *sd* shell within the *jj* coupling scheme. In their multichannel calculation, Langanke *et al.* introduce an excited 0^+ state of ^{18}O while our study takes account of the $^{18}O(2^+)$ first excited state.

After discussing the ^{22}Ne spectrum, we aim at suggesting spin assignments for low-lying states in the mirror nucleus ^{22}Mg. Although this nucleus has been recently investigated[9] experimentally, its level scheme remains poorly known. Our model provides Coulomb shifts which are expected to be reliable since the Coulomb interaction is treated exactly. The last point of this paper concerns the $^{18}O(\alpha,\gamma)^{22}Ne$ capture reaction. The level scheme of ^{22}Ne has been experimentally studied[10] near the $\alpha + {}^{18}O$ threshold. However, spin assignments remain sometimes uncertain. Moreover, the nonresonant contribution at low energies is based on a very simple approach of the direct-capture process.[10] For these reasons, the $^{18}O(\alpha,\gamma)^{22}Ne$ reaction rate recommended for astrophysical applications presents important uncertainties.[11]

The paper is organized as follows. In Sec. II we present briefly the microscopic model by emphasizing on the three-cluster structure of the wave functions. In Sec. III we present a new method for deriving the energies and widths of resonances. Section IV is devoted to the study of the ^{22}Ne spectrum; the band structure and the electromagnetic transition probabilities are discussed with respect to the available experimental data; we also determine the Coulomb shifts between the ^{22}Ne and ^{22}Mg states. In Sec. V we give the microscopic $^{18}O(\alpha,\gamma)^{22}Ne$ capture cross section, and provide a simple parametrization of the nonresonant reaction rate. Concluding remarks are presented in Sec. VI.

II. THE THREE-CLUSTER MODEL

The microscopic wave function with total spin J and parity π of the 22 nucleon system is defined in the GCM as

 ©1988 The American Physical Society

$$\Psi^{JM\pi}=\sum_{lL}\mathcal{A}\phi_\alpha\phi_{^{16}O}\phi_{2n}[Y_l(\Omega_\rho)\otimes Y_L(\Omega_{\rho'})]^{JM}G_{lL}^{J\pi}(\rho,\rho') , \quad (1)$$

where $\mathcal{A}$ is the antisymmetrization projector, ρ is the relative coordinate between the α and ^{18}O clusters, and ρ' between ^{16}O and dineutron. The internal wave functions $\phi_\alpha,\phi_{^{16}O}$, and ϕ_{2n}, of the α, ^{16}O, and dineutron clusters are defined in the harmonic-oscillator model. In (1), l is the angular momentum relative to ρ and L relative to ρ'. In the GCM, the function $G_{lL}^{J\pi}(\rho,\rho')$ is written as

$$G_{lL}^{J\pi}(\rho,\rho')=\int F_{lL}^{J\pi}(R_1,R_2)\Gamma_l(b_1,\rho,R_1)\times\Gamma_L(b_2,\rho',R_2)dR_1dR_2 , \quad (2)$$

where $F_{lL}^{J\pi}$ is the generator function depending upon the generator coordinates R_1 and R_2. The parameters b_1 and b_2 are given in the present case by $b_1=(\frac{11}{36})^{1/2}b$ and $b_2=(\frac{9}{16})^{1/2}b$ where b is the oscillator parameter common to all clusters. Function Γ_l is a projected displaced Gaussian function (see Ref. 4). With (2), the total wave function (1) can be written as a linear combination of projected Slater determinants $\Phi_{lL}^{JM\pi}$, yielding

$$\Psi^{JM\pi}=\sum_{i,j}F_{lL}^{J\pi}(R_{1i},R_{2j})\Phi_{lL}^{JM\pi}(R_{1i},R_{2j}) , \quad (3)$$

where the integrals in (2) have been replaced by finite sums over two sets of generator coordinates. We have shown in Ref. 4 that the calculation of the matrix elements between projected Slater determinants involves five-dimensional integrals which represent an enormous increase of calculation times with respect to the two-cluster model.

Let us now consider the ^{18}O wave function

$$\phi_{^{18}O}^{Lm\omega}=\mathcal{A}\phi_{^{16}O}\phi_{2n}\tilde{g}^{L\omega}(\rho')Y_L^m(\Omega_{\rho'}) , \quad (4)$$

where $\tilde{g}^{L\omega}(\rho')$ is a radial wave function between the ^{16}O and dineutron clusters determined by the 18 nucleon Hamiltonian, and ω denotes the level of excitation in the relative motion. According to Ref. 4, the three-cluster wave function (2) can be expanded as

$$G_{lL}^{J\pi}(\rho,\rho')=\sum_\omega g_{lL\omega}^{J\pi}(\rho)\tilde{g}^{L\omega}(\rho') , \quad (5)$$

which allows one to write (1) as

$$\Psi^{JM\pi}=\sum_{lL\omega}\mathcal{A}\phi_\alpha[Y_l(\Omega_\rho)\otimes\phi_{^{18}O}^{L\omega}]^{JM}g_{lL\omega}^{J\pi}(\rho) . \quad (6)$$

The three-cluster problem is therefore replaced by a multichannel two-center model where the radial functions $g_{lL\omega}^{J\pi}(\rho)$ are determined by the Hamiltonian of the 22-nucleon system. In the GCM notation, one has

$$\Psi^{JM\pi}=\sum_{lL\omega i}f_{lL\omega}^{J\pi}(R_{1i})\tilde{\Phi}_{lL\omega}^{JM\pi}(R_{1i}) , \quad (7)$$

where $f_{lL\omega}^{J\pi}$ and $\tilde{\Phi}_{lL\omega}^{JM\pi}$ are, respectively, a new generator function and a combination of Slater determinants, depending on the R_1 coordinate only.[4]

The microscopic Hamiltonian contains the Volkov V_2 force and the exact Coulomb interaction. The oscillator parameter b is chosen equal to 1.8 fm. The ^{18}O wave functions are defined with a single generator coordinate $R_2=1.8$ fm. This restriction to a single generator coordinate has been shown[5] in the $\alpha+^{20}$Ne case to be accurate enough for the description of ^{24}Mg in the three-cluster model. A similar conclusion is expected here as far as the clustering is weaker in ^{18}O than in the $\alpha+^{16}$O system. The 0^+ ground state and 2^+ first excited state of ^{18}O are included in the calculation. The Majorana parameter of the nucleon-nucleon interaction is chosen as $M=0.6155$ for positive-positive states, and $M=0.6166$ for negative-parity states. These values are determined by fitting the experimental energies of ^{22}Ne states presenting a marked $\alpha+^{18}$O structure (see below), and therefore well described by the model. Notice the very small difference between both values of the Majorana parameters. This indicates that the parity effect in ^{22}Ne is well reproduced. With our parameter choice, the excitation energy of the ^{18}O(2^+) state is about 0.9 MeV for both parities, which is somewhat too low with respect to the experimental value[12] (1.98 MeV). Let us remark that our model does not include the ^{21}Ne$+n$ channel, that is open 0.70 MeV above the $\alpha+^{18}$O threshold. The main reason is that a ^{21}Ne wave function cannot easily be defined in the present approach. However, since the neutron channel presents a strongly repulsive centrifugal barrier, it is not expected to influence significantly the ^{22}Ne wave functions when the angular momentum is different from 0.

III. DERIVATION OF REDUCED WIDTHS

We have shown in Ref. 13 that the width of a narrow resonance can be estimated in the bound-state approximation (BSA). This method assumes a Gaussian behavior of the wave function for large interdistances between the clusters. Here, we aim at presenting a new method which goes beyond the BSA, and gives more accurate values even in multichannel calculations. We start from the Bloch-Schrödinger equation[14]

$$(H+\mathcal{L}(\mathbf{L})-E^{J\pi})\Psi^{JM\pi}=\mathcal{L}(\mathbf{L})\Psi^{JM\pi} , \quad (8)$$

where $\mathcal{L}(\mathbf{L})$ is the Bloch operator, depending on a set of L values which can be chosen freely. Equation (8) is solved in the microscopic R-matrix (MRM) framework.[15] In this method, the configuration spaced is divided in two regions: an internal one (of radius a) where the antisymmetrization between the colliding nuclei is taken into account, and an external one, where the antisymmetrization and the nuclear interaction are negligible. Accordingly, the wave function (7) is given by (3) in the internal region; in the external region, $\mathcal{A}$ can be removed and the asymptotic behavior of $g_{lL\omega}^{J\pi}(\rho)$ in (6) is given by Eq. (4) of Ref. 14. We have shown in that work that a convenient choice for the L values is

$$L=kaO_l'(ka)/O_l(ka)$$

or

$$L=2kaW'_{-\eta,l+(1/2)}(2ka)/W_{-\eta,l+(1/2)}(2ka)$$

according to whether the channel is open or closed. In these equations, O_l is an outgoing Coulomb function, and

W is a Wittakher function; η is the Sommerfeld parameter and k is the wave number. As it has been shown in Ref. 14, the resonance and bound-state energies correspond to the eigenvalues of the equation

$$\mathcal{L}(\mathbf{L})\Psi^{JM\pi}=0 \ . \tag{9}$$

Using (7) and (8) yields

$$\sum_{ilL\omega} d^{J\pi}_{lL\omega i}\langle \tilde{\Phi}^{JM\pi}_{lL\omega}(R_{1i}) \mid H+\mathcal{L}(\mathbf{L}) - \varepsilon^{J\pi} \mid \tilde{\Phi}^{JM\pi}_{l'L'\omega'}(R_{1i'})\rangle_P = 0 \ , \tag{10}$$

where the index P means that the equation is solved on the internal region.[15] This equation is nonlinear since the constants L depend on energy. In practice, one solves (10) iteratively by starting with all constants L equal to zero. The convergence is reached after a small number of iterations. Equation (10) has been established in Ref. 16 for bound states; it is extended here to resonances. In this case, the eigenvalues of (10) are complex since the Bloch constants at a positive energy contain an imaginary part. The energy and the width of a resonance are given by

$$\begin{aligned} E^{J\pi} &= \mathrm{Re}(\varepsilon^{J\pi}) \ , \\ \Gamma^{J\pi} &= -2\,\mathrm{Im}(\varepsilon^{J\pi}) \ . \end{aligned} \tag{11}$$

The sign minus in the definition of the width arises from the present choice of the L constants. The wave function at a resonance is obtained from (6) where the radial part reads[14]

$$g^{J\pi}_{lL\omega,\mathrm{res}}(\rho)=[256\pi^5/(2l+1)]^{1/2}\sum_i d^{J\pi}_{lL\omega i}\Gamma_l(b_1,\rho,R_{1i}) \ . \tag{12}$$

Equation (12) leads to the definition of the reduced width in the channel lL

$$(\gamma^{J\pi}_{lL})^2=(\hbar^2 a/2\mu)\mid g^{J\pi}_{lL\omega,\mathrm{res}}(a)\mid^2 \ , \tag{13}$$

where μ is the reduced mass. This expression holds for resonances as well as for bound states. The method presented here improves the method of Ref. 14, where the background contribution to the collision matrix is neglected. We have tested the validity of (13) by comparing the values of the widths with a Breit-Wigner parametrization of the collision matrix. The determination of the partial widths in a multichannel calculation from a Breit-Wigner parametrization is not easy. The method proposed here provides straightforwardly these quantities, with remarkable accuracy. The MRM radius chosen here is 9 fm. Such a large value is necessary for systems involving a *sd* nucleus.[5] The physical quantities such as the energy and width of a resonance are nearly insensitive to this radius provided that it is large enough to render negligible the nuclear interaction and the antisymmetrization effects between the colliding nuclei.

IV. BOUND-STATE AND RESONANCE PROPERTIES OF ^{22}Ne AND ^{22}Mg

A. Band structure of ^{22}Ne

The different states obtained in the $\alpha+^{18}\mathrm{O}(0^+,2^+)$ model are gathered in Tables I (positive parity) and II (negative parity). The reduced α widths calculated at $a=9$ fm are presented as

$$\theta^2_L=\sum_l \gamma^2_{lL}/\gamma^2_W \ , \tag{14}$$

i.e., in units of the Wigner limit γ^2_W. For the sake of comparison with experiment, we present the GCM values of E_x, deduced from the c.m. energies by adding the experimental threshold (9.67 MeV). A band is formed by states presenting similar reduced α widths, and enhanced $E2$ transition probabilities between them (see below). The band structure is summarized in Figs. 1 and 2. Let us now discuss each band.

The 0^+_1 band. This well-known band has too small a rotational constant in the GCM. This indicates that the model slightly overestimates the clustering in the ground-state band. Therefore, high-spin states are located significantly too low. This band can be described in a single-channel approach,[7] but the reduced α widths presented in Table I show that the mixing between the $\alpha+^{18}\mathrm{O}(0^+)$ and $\alpha+^{18}\mathrm{O}(2^+)$ configurations is not negligible.

The 2^+ band. This band has mainly an $\alpha+^{18}\mathrm{O}(2^+)$ structure, as it is suggested by the reduced α widths. As for the ground-state band, the GCM overestimates the binding energies. The origin of this overestimation is most likely due to the lack of saturation of the ^{18}O nucleus and of the α particle. Because of the equal oscillator parameter assumption for the ^{16}O, dineutron and α clusters, the $\alpha+^{18}$O threshold is underestimated. This problem is well known in the $\alpha+^{12}$C system,[14] for example, and leads to too strong a binding energy for the unified system. The assignment of the 2^+ (4.46 MeV), 3^+ (5.64 MeV), and 4^+ (6.35 MeV) to the 2^+ band is well established.[18] Broude *et al.*[18] propose the 7.41 MeV level as candidate for the 5^+ state. However, if one keeps in mind the theoretical underestimation of about 2 MeV on the binding energies, we rather suggest the 9.61 MeV level whose spin is well established, as experimental counterpart for the 5^+ state. The GCM predicts 6^+, 7^+, and 8^+ states which should be located respectively near 12, 14, and 16 MeV.

The 1^+ band. The model suggests the existence of a 1^+ band, built on the 5.34 MeV level, and whose rotational constant is smaller than the one of the 2^+ band (see Fig. 1). The reduced α widths presented in Table I favor an $\alpha+^{18}\mathrm{O}(2^+)$ structure for this band. Our study suggests to assign the 7.31 MeV level, whose spin is 3 or 4 and whose parity is positive,[18] to the 3^+ state of this band. The theoretical 5^+ state might be identified to the 7.41 MeV level,[18] whose spin is 3 or 5 and whose parity is positive. The model predicts 6^+, 7^+, and 8^+ states whose experimental counterparts should be located around 8, 9, and 11 MeV, respectively. The 8^+ state

TABLE I. Energies and reduced α widths (in %) of ^{22}Ne positive-parity states.

J^π	E_x^{exp}	$E_{c.m.}^{GCM}$	E_x^{GCM}	θ_0^2	θ_2^2	Ref.
			$K^\pi=0_1^+$			
0^+	0.0	−10.45	−0.78	2.2×10^{-5}	5.5×10^{-5}	17
2^+	1.27	−9.69	−0.02	4.0×10^{-5}	6.6×10^{-5}	17
4^+	3.35	−8.24	1.43	5.3×10^{-5}	5.0×10^{-5}	17
6^+	6.31	−6.17	3.50	4.8×10^{-7}	1.2×10^{-4}	17
8^+	11.00	−2.95	6.72	3.4×10^{-4}	3.8×10^{-4}	18
			$K^\pi=2^+$			
2^+	4.46	−7.41	2.26	2.1×10^{-6}	1.5×10^{-4}	17
3^+	5.64	−6.37	3.30		3.1×10^{-4}	17
4^+	6.31	−5.06	4.61	6.0×10^{-5}	8.0×10^{-4}	17
5^+	9.61	−3.45	6.22		7.9×10^{-4}	18
6^+		−0.72	8.95	4.1×10^{-4}	4.4×10^{-3}	
7^+		1.04	10.71		2.2×10^{-3}	
8^+		3.73	13.40	5.6×10^{-4}	1.0×10^{-3}	
			$K^\pi=1^+$			
1^+	5.34	−6.32	3.35		2.3×10^{-4}	17
2^+	5.36	−6.96	2.61	4.9×10^{-5}	3.8×10^{-4}	17
3^+	7.31	−5.84	3.83		1.6×10^{-4}	18
4^+	5.52	−6.04	3.63	9.1×10^{-5}	7.4×10^{-4}	17
5^+	7.41	−4.62	5.05		1.1×10^{-4}	18
6^+		−4.02	5.65	1.4×10^{-3}	2.2×10^{-3}	
7^+		−2.49	7.18		3.6×10^{-4}	
8^+		−0.74	8.93	4.1×10^{-3}	3.6×10^{-3}	
			$K^\pi=0_2^+$			
0^+	6.24	−5.30	4.37	1.7×10^{-3}	3.7×10^{-4}	17
2^+	7.64	−3.25	6.42	2.9×10^{-3}	5.3×10^{-4}	17
4^+	9.64	−1.50	8.17	3.5×10^{-3}	1.7×10^{-3}	19
6^+	10.41	0.43	10.10	2.1×10^{-3}	9.3×10^{-4}	18
			$K^\pi=0_3^+$			
0^+	10.28	0.61	10.28	3.5	0.4	10
2^+	10.86	1.25	10.92	2.9	1.2	10
4^+		2.55	12.22	1.0	5.9	
6^+		4.56	14.23	0.3	15.4	

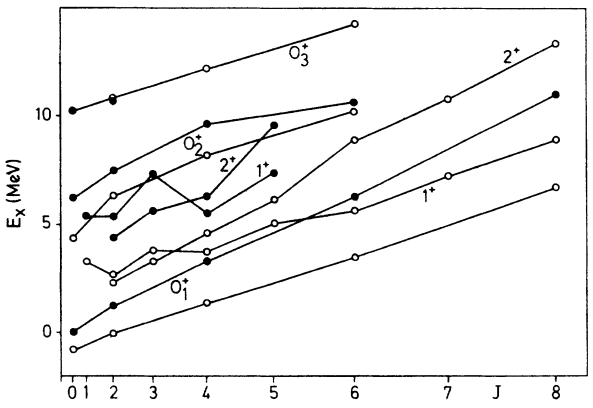

FIG. 1. Band structure for positive-parity states in ^{22}Ne. The GCM states are represented by open circles, and the suggested experimental counterparts by black circles.

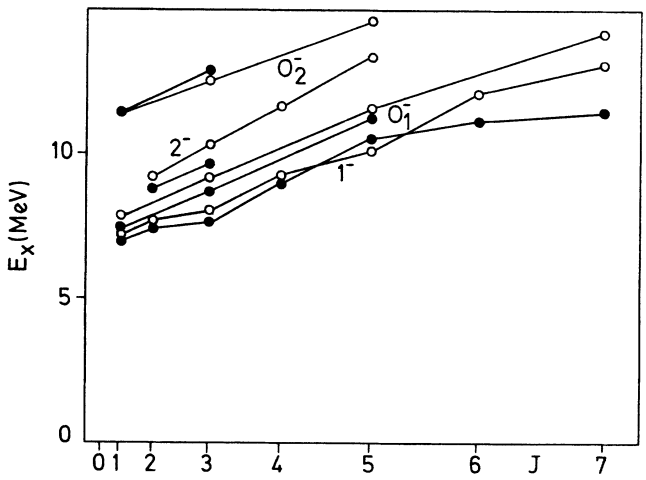

FIG. 2. See Fig. 1 for negative-parity states.

TABLE II. Energies and reduced α widths (in %) of ^{22}Ne negative-parity states.

J^π	E_x^{exp}	$E_{c.m.}^{GCM}$	E_x^{GCM}	θ_0^2	θ_2^2	Ref.
			$K^\pi=0_1^-$			
1^-	7.49	−1.86	7.91	0.14	0.05	17
3^-	8.74	−0.43	9.24	0.23	0.06	17
5^-	10.75	2.04	11.71	0.34	0.14	10
7^-		4.60	14.27	0.14	0.21	
			$K^\pi=1^-$			
1^-	7.05	−2.36	7.31	0.07	0.07	17
2^-	7.66	−1.85	8.05		0.13	17
3^-	7.72	−1.62	7.82	0.02	0.13	17
4^-	9.07	−0.31	9.36		0.18	19
5^-	10.61	0.31	10.08	0.01	0.21	10
6^-	11.11	2.50	12.17		0.27	18
7^-	11.48	3.36	13.13	9.7×10^{-4}	0.54	18
8^-		6.53	16.20		0.64	
			$K^\pi=0_2^-$			
1^-	11.47	1.80	11.47	0.60	2.1	10
3^-	12.88	2.91	12.58	0.42	5.5	17
5^-		5.10	14.77	0.22	14.4	
			$K^\pi=2^-$			
2^-	9.10	−0.51	9.16		0.21	17
3^-	9.64	0.65	10.32	0.03	0.28	19
4^-		2.25	11.82		0.35	
5^-		3.70	13.37	0.01	1.3	

might be identified to the 11.13 MeV level observed by Trautvetter *et al.*[10]

The 0_2^+ band. Like in the ^{24}Mg nucleus,[5] the theoretical model gives rise to an excited 0_2^+ band whose head is located below the $\alpha+^{18}$O threshold. The 0^+ and 2^+ theoretical states are unambiguously assigned to the 6.24 and 7.64 MeV experimental levels,[17] while a valuable candidate for the 4^+ state has been observed by Szanto *et al.*[19] at 9.64 MeV. The 6^+ state might be identified to the experimental 10.41 MeV state[19] whose spin is 6 or 8.

The 0_3^+ band. This excited band is located close to the Coulomb barrier. Its band head has a marked $\alpha+^{18}$O(0^+) structure as revealed by the reduced α widths. Let us notice that, for a channel radius lower than 9 fm, the reduced α width is significantly increased (for example, at 6 fm one gets $\theta_0^2=67\%$). The band head is assigned to the 10.28 MeV state for which a $J^\pi=0^+$ assignment is most likely.[10] This state will play an important role in the ^{18}O$(\alpha,\gamma)^{22}$Ne capture reaction. Let us point out that the upper limit quoted in Ref. 10 for its total width (2 keV) is obviously overestimated. Since the 0^+ (10.28 MeV) state is located below the $n+^{21}$Ne threshold, its width is nearly equal to the α width. Using the experimental upper limit for the α width leads to a reduced width (at 6 fm) of more than 6.10^4 times the Wigner limit. In view of its energy, the GCM 2^+ state can be assigned to the 10.86 MeV state, whose spin is lower than 4^+ (see Ref. 10). The 4^+ and 6^+ levels of this band are aligned with the 0^+ and 2^+ states in a $J(J+1)$ diagram (see Fig. 1), with a rotational constant of 94 keV. Since the locations of the 0^+ and 2^+ states are in fair agreement with experiment, one could expect a similar property for the 4^+ and 6^+ states. Therefore, the prediction of a 4^+ (12.12 MeV) and a 6^+ (14.23 MeV) states should be considered as reliable. A striking property of the reduced α widths in the 0_3^+ band is observed in Table I. The θ_0^2 values systematically decrease when J increases, while the θ_2^2 values increase. This can be explained as follows. For each excited states, the orbital momentum in the $\alpha+^{18}$O(0^+) channel is $l=J$ and the lowest value in the $\alpha+^{18}$O(2^+) channel is $l=|J-2|$. Since the excited configuration presents a small threshold energy, the effective barrier (Coulomb plus centrifugal terms) in the $\alpha+^{18}$O(2^+) configuration is shifted below the effective barrier of the $\alpha+^{18}$O(0^+) configuration when the spin increases. The states of the 0_3^+ band being located close to their effective barrier, the reduced α widths in the $\alpha+^{18}$O(2^+) configuration increase with increasing values of J.

The 0_1^- band. The 3^- state of this band is the second 3^- state found in the GCM (see the discussion of the 1^- band below). Therefore, the assignment of the experimental 3^- (8.74 MeV) state is most likely; this is also supported by the good agreement between theory and experiment for the energy. In view of the $1^- - 3^-$ theoretical gap, the 1^- (7.49 MeV) experimental state can be considered as a good candidate for the 0_1^- band head. A 5^- state has been observed by Trautvetter *et al.*[10] at 10.75 MeV and could belong to the 0_1^- band. Our calculation predicts a 7^- resonance located near 14 MeV with a α width of about 1 keV.

The 1^- band. This band is characterized by reduced α

widths larger in the $\alpha+^{18}O(2^+)$ channel than in the $\alpha+^{18}O(0^+)$ configuration. Its states can be accordingly considered as $\alpha+^{18}O(2^+)$ bound states. As it is seen from Table II and Fig. 2, valuable experimental candidates exist up to $J^\pi=7^-$. From the energy difference between the 1^- states of the 0_1^- and 1^- bands, the experimental 7.05 MeV level can be considered as a valuable counterpart for the band head. The 2^- and 3^- states are unambiguously assigned to the 7.66 MeV and 7.72 MeV levels, respectively.[17] A 4^- state has been observed by Szanto *et al.*[19] at 9.07 MeV, an energy close to the theoretical one. The theoretical 5^- state is probably the 5^- level proposed by Trautvetter *et al.*[10] at 10.61 MeV. Broude *et al.*[18] have identified two levels at 11.11 and 11.48 MeV. The former has a spin 6^-, 7^+, or 8 and the latter 7. According to their energies, these states might be assigned to the theoretical 6^- and 7^- levels of the 1^- band.

The 0_2^- band. This band presents a strong clustering, as indicated by the large reduced widths in the $\alpha+^{18}O(2^+)$ channel. The 1^- state is identified to the 11.47 MeV experimental state, which presents an important γ width for transition towards the ground state,[10,20] in agreement with our investigation (see Sec. IV C). According to its energy, the 3^- resonance can be assigned to the experimental 12.88 MeV state[17] which is observed in the $^{18}O(\alpha,\alpha)^{18}O$ and $^{18}O(\alpha,n)^{21}Ne$ channels. The 5^- theoretical state follows a rotational law (see Fig. 2) and its location is predicted near 15 MeV.

The 2^- band. The model gives rise to a 2^- band whose head is located near 9 MeV. Consequently, the 9.10 MeV state[17] whose spin is 1^-, 2^-, or 3^- might be a good candidate for this level. A state with spin 3 or 4 has been observed by Szanto *et al.*[19] at 9.64 MeV, and could be assigned to the 3^- state of the 2^- band. The GCM predicts 4^- and 5^- states located, respectively, near 12 and 13 MeV.

B. The $^{18}O(\alpha,\alpha)^{18}O(0^+)$ and $^{18}O(\alpha,\alpha)^{18}O(2^+)$ scatterings

In Figs. 3 and 4 we present the $^{18}O(\alpha,\alpha)^{18}O$ collision matrices. They are parametrized by

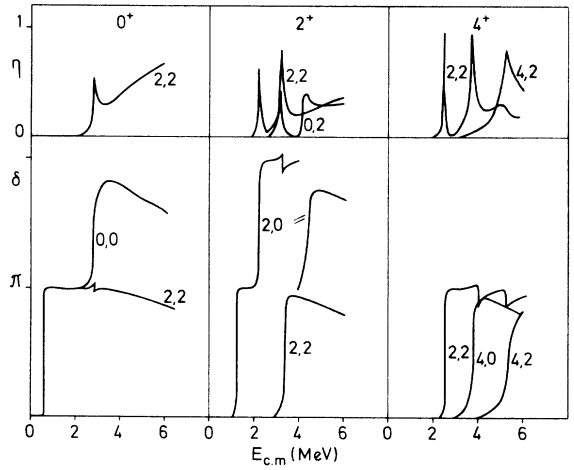

FIG. 3. Positive-parity collision matrices (15) as a function of the c.m. energy; the curves are labeled by the indexes $l'L'$ (see Sec. IV B).

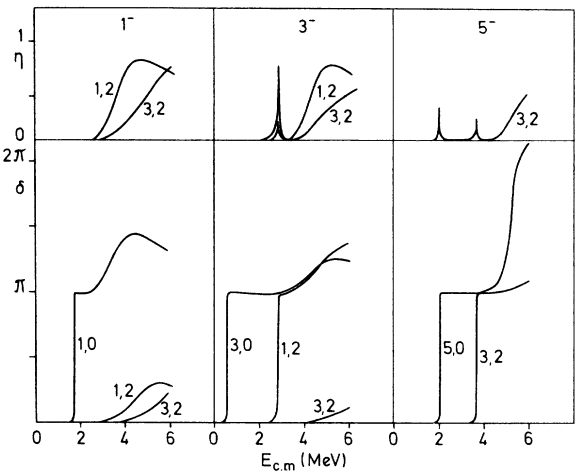

FIG. 4. See Fig. 3 for negative parity.

$$U^{J\pi}_{lL,l'L'}=\eta^{J\pi}_{lL,l'L'}\exp(2i\delta^{J\pi}_{lL,l'L'}) , \tag{15}$$

where $\eta^{J\pi}$ and $\delta^{J\pi}$ are real. In Figs. 3 and 4 only the diagonal phase shifts $\delta^{J\pi}$ (corresponding to $l=l'$ and $L=L'$) are presented. For the transmission coefficient $\eta^{J\pi}$, we select $L=0$, $l=J$. The values of l' and L' are indicated on the curves. In Table III we give the energies and widths deduced from (11). For $J^\pi=0^+$, the phase shift presents a sharp variation near 2.8 MeV. This resonance can be assigned to the 0^+ ($E_{c.m.}=2.59$ MeV) state observed experimentally.[17] The theoretical and experimental (70 keV) widths are in fair agreement. The 2^+ phase shifts present several resonances in addition to the states classified in the band structure discussed in Sec. IV A. The theoretical state at $E_{c.m.}=2.2$ MeV is a valuable candidate for the experimental 2.02 MeV resonance whose width (9 keV) is in nice agreement with our result. From its location and width, we suggest that the theoretical 3.2 meV resonance has been observed at 3.14 MeV. The calculation predicts two 4^+ resonances located near 3.7 and 5.4 MeV, which have not been observed experimentally.

The negative-parity phase shifts present a broad barrier resonance for $J^\pi=1^-$ and 3^-. When the spin increases, the coupling between the elastic and inelastic

TABLE III. Energies and widths of resonances in $^{18}O(\alpha,\alpha)^{18}O$ scattering.

J^π	$E^{GCM}_{c.m.}$	Γ_0	Γ_2	$E^{exp}_{c.m.}$
0^+	2.8	0.16	0.01	2.59
1^-	~3.5	~1	~0	
2^+	2.2	1.3×10^{-2}	1.6×10^{-3}	2.02
	3.2	3.0×10^{-2}	7.8×10^{-2}	3.14
	4.3	0.11	1.2×10^{-4}	
3^-	2.9	2.7×10^{-3}	1.4×10^{-2}	3.19
	~4.5	~1	~1	
4^+	3.7	0.09	0.06	
	5.4	0.10	0.36	
5^-	5.2	3.2×10^{-3}	0.24	

TABLE IV. $E1$ reduced transition probabilities in ^{22}Ne in W.u.

$J_i^{\pi_i}$	$J_f^{\pi_f}$	$B(E1)$	Γ_γ (eV)
		$K^\pi=0_1^- \rightarrow K^\pi=0_1^+$	
1^-	0^+	2.4×10^{-6}	8.1×10^{-4}
	2^+	4.9×10^{-4}	0.13
3^-	2^+	3.2×10^{-3}	1.35
	4^+	9.1×10^{-4}	0.23
		$K^\pi=0_1^- \rightarrow K^\pi=2^+$	
1^-	2^+	6.2×10^{-4}	0.06
3^-	2^+	1.9×10^{-3}	0.34
	3^+	1.9×10^{-3}	0.21
	4^+	1.2×10^{-2}	1.10
		$K^\pi=0_1^- \rightarrow K^\pi=0_2^+$	
1^-	0^+	7.8×10^{-3}	0.17
	2^+	1.3×10^{-2}	0.16
3^-	2^+	1.4×10^{-2}	0.16
	4^+	6.9×10^{-3}	4.1×10^{-3}
		$K^\pi=0_2^- \rightarrow K^\pi=0_1^+$	
1^-	0^+	1.0×10^{-2}	9.8
	2^+	8.7×10^{-3}	6.9
3^-	2^+	1.5×10^{-3}	1.5
	4^+	4.5×10^{-4}	0.3

channels becomes more important, and these broad resonances disappear. The 1^- and 3^- resonances have a location and a width similar to these obtained in the single-channel calculation of Langanke.[7] In addition to these broad resonances, we obtain a 3^- resonance at 2.9 MeV, which can be assigned to the 3.19 MeV experimental state. The GCM also suggests a 5^- resonance near $E_{\text{c.m.}}=5.2$ MeV.

C. Electromagnetic transition probabilities in ^{22}Ne

The $E1$ and $E2$ reduced transition probabilities, expressed in Weisskopf units (W.u.) are presented in Tables IV–VI. The $M1$ operator gives rise to vanishing matrix elements because of the closed-shell character of the nuclei involved in the present three-cluster model.[16] Let us first discuss the $B(E1)$ displayed in Table IV. The radiation width for the 1^- (7.49 MeV) state towards the ground state is found very small. We suggest that this state decays to the 2^+ or 0_2^+ band preferentially. The γ widths for transitions between the 0_2^- and 0_1^+ bands are significantly stronger. The $B(E1)$ from the 1^- (11.48 MeV) state of the 0_2^- band to the ground-state band has been measured by Chouraqui *et al.*[20] and by Trautvetter *et al.*[10] Both investigations agree for giving strong transition probabilities. However, the values quoted in these references are significantly different ($\Gamma_\gamma=0.16\pm0.02$ eV in Ref. 10 and $\Gamma_\gamma=0.9\pm0.2$ eV in Ref. 20). The still larger value obtained in the present model probably arises from the lack of reaction channels. We have shown in Ref. 6 that the introduction of excited configurations reduces the $E1$ matrix elements, especially for strongly clustered states like the 1^- (11.48 MeV) state. In the present case, it is most likely that the introduction of the $n+{}^{21}$Ne or other $\alpha+{}^{18}$O* configurations would reduce the γ width of this state.

The $E2$ transition probabilities presented in Table V are in fair agreement with the available experimental data. Let us point out that no effective charge is employed in the present calculation. The experimental lower limit for the $8^+\rightarrow6^+$ transition in the ground-state band seems largely underestimated. For transitions in a $K=0$ band, the $B(E2)$ follow qualitatively the law[22]

$$B(E2,J\rightarrow J-2)\approx\frac{5}{16\pi}Q_0^2\frac{J(J+1)}{4J^2-1}\ , \tag{16}$$

where Q_0 is an intrinsic quadrupole moment almost constant in a band. It is easy to show that Q_0 can be approximately related to the mean distance $\langle\rho^2\rangle^{1/2}$ between the clusters by

$$Q_0\approx2\left[Z_1\left[\frac{A_2}{A}\right]^2+Z_2\left[\frac{A_1}{A}\right]^2\right]\langle\rho^2\rangle\ . \tag{17}$$

In the ground-state band, the $B(E2)$ values nearly correspond to $\langle\rho^2\rangle^{1/2}=3.3$ fm, which is smaller than the sum of the α and ^{18}O radii (≈4.6 fm). This indicates a weak clustering in the ground-state band. Let us recall that this theoretical clustering is probably still too important, according to the GCM rotational constant of the band (see Sec. IV A). The transitions in the 2^+ band are significantly stronger than between the 2^+ and 0_1^+ bands. For these transitions, the agreement between theory and experiment is quite acceptable. In the 0_2^+ band, the $\langle\rho^2\rangle^{1/2}$ values resemble the ones of the ground-state band; the 0_2^+ band can therefore be interpreted as a weakly clustered band. On the contrary, the mean distance between the clusters in the 0_3^+ band is nearly equal to 5.2 fm, indicating an important clustering since this value is larger than the sum of the internal radii. Transitions between the 0_3^+ and 0_1^+ bands correspond to small $B(E2)$, but the large energy differences make the γ widths of the order of 1 eV.

The $B(E2)$ between negative-parity states are presented in Table VI. In the 0^- band, the $E2$ reduced transition probabilities lead to a Q_0 value of about 50 $e$fm^2, which corresponds to a $\langle\rho^2\rangle^{1/2}$ value of 4 fm. The clustering is therefore expected to be more important in this band than in the ground-state band. Table VI confirms that transitions inside a band are stronger than transitions between two different bands. The 0_2^- band presents a mean distance between the clusters of about 4.7 fm, which is similar to the sum of the ^{18}O and α radii. Hence the 0_2^- band can be considered as a molecular $\alpha+{}^{18}$O band.

TABLE V. $E2$ reduced transition probabilities (in W.u.) between ^{22}Ne positive-parity states.

$J_i^{\pi_i}$	$J_f^{\pi_f}$	$B(E2)_{GCM}$	Γ_γ (meV)	$B(E2)_{exp}$	Ref.
			$K^\pi=0_1^+ \rightarrow K^\pi=0_1^+$		
2^+	0^+	8.4	6.3×10^{-3}	1.36 ± 1.6	17
4^+	2^+	9.5	0.18	$20.1^{+4.3}_{-3.0}$	10
6^+	4^+	10.2	1.1	$12.8^{+3.1}_{-2.1}$	10
8^+	6^+	7.9	8.1	≥ 0.02	10
			$K^\pi=2^+ \rightarrow K^\pi=2^+$		
3^+	2^+	18.5	6.6×10^{-2}		
4^+	2^+	4.9	1.0		
5^+	4^+	6.4	0.20		
6^+	4^+	6.4	29.6		
7^+	6^+	1.6	7.8×10^{-2}		
			$K^\pi=2^+ \rightarrow K^\pi=0_1^+$		
2^+	0^+	5.5×10^{-2}	4.2×10^{-2}		
2^+	2^+	0.30	5.4×10^{-2}	>0.3	21
3^+	2^+	0.16	0.19	>0.05	21
4^+	2^+	0.70	4.4		
			$K^\pi=0_2^+ \rightarrow K^\pi=0_2^+$		
2^+	0^+	5.9	0.64		
4^+	2^+	7.1	0.36		
6^+	4^+	6.5	0.52		
			$K^\pi=0_2^+ \rightarrow K^\pi=0_1^+$		
2^+	0^+	7.0×10^{-4}	4.0×10^{-2}		
0^+	2^+	2.0×10^{-2}	9.5×10^{-2}		
2^+	2^+	5.7×10^{-3}	0.19		
4^+	2^+	4.2×10^{-2}	4.7		
			$K^\pi=0_3^+ \rightarrow K^\pi=0_3^+$		
2^+	0^+	41.1	1.4×10^{-2}		
4^+	2^+	50.3	5.5×10^{-1}		
			$K^\pi=0_3^+ \rightarrow K^\pi=0_1^+$		
2^+	0^+	0.73	474		
0^+	2^+	2.8	960		
2^+	2^+	0.86	397		
4^+	2^+	0.91	738		

D. ^{22}Mg spectrum

Although the ^{22}Mg spectrum has been recently investigated by Alford *et al.*,[9] some uncertainties remain on the spin assignments. The present study offers a powerful way for a ^{22}Mg investigation, since it provides Coulomb shifts based on the exact two-body Coulomb interaction. By comparing these quantities with the ^{22}Ne energies, it is possible to predict accurately the spectrum of low-lying states of ^{22}Mg. In Table VII the Coulomb shifts ΔE_{GCM} are given by

$$\Delta E_{GCM}=E(^{22}\text{Mg})-E(^{22}\text{Ne})-E(^{18}\text{Ne})+E(^{18}\text{O}) , \quad (18)$$

where all energies are theoretical. The energies of ^{22}Mg are calculated similarly to those of ^{22}Ne. The predicted ^{22}Mg energies are deduced from

$$E_x^{\text{predicted}}=E_x^{\text{exp}}(^{22}\text{Ne})+\Delta E_{GCM}-\Delta E_{GCM}(\text{g.s.}) . \quad (19)$$

Table VII shows that the GCM Coulomb shifts succeed in reproducing the observed energies of the low-lying states in the ground-state band. In the 2^+ band, the natural parity states are reproduced reasonably well. We suggest 3^+ and 5^+ states near 5.6 and 9.6 MeV, respectively. The head of the 1^+ band is predicted at 5.34 MeV. This excitation energy is in nice agreement with the 5.32 MeV state whose spin is controverted. Endt and van der Leun[17] suggest a spin 1, 2, or 3, while Alford *et al.*[9] propose a relative orbital momentum 4. Our calculation supports a 1^+ assignment, which is consistent with the data of Ref. 17. The 2^+ and 4^+ energies found in the model have valuable experimental counterparts.[17] Notice that the 1^+, 2^+, and 4^+ state are not resolved in

TABLE VI. $E2$ reduced transition probabilities (in W.u.) between ^{22}Ne negative-parity states.

$J_i^{\pi_i}$	$J_f^{\pi_f}$	$B(E2)$	Γ_γ (meV)
	$K^\pi=0_1^- \rightarrow K^\pi=0_1^-$		
3^-	1^-	20.6	0.37
5^-	3^-	27.5	7.5
7^-	5^-	17.2	5.7
	$K^\pi=1^- \rightarrow K^\pi=1^-$		
2^-	1^-	15.5	1.5×10^{-3}
3^-	1^-	17.5	1.1×10^{-2}
3^-	2^-	17.2	3.5×10^{-5}
4^-	2^-	22.2	5.7×10^{-1}
	$K^\pi=0_1^- \rightarrow K^\pi=1^-$		
1^-	1^-	24.6	2.1×10^{-3}
3^-	1^-	4.9	3.9×10^{-1}
3^-	2^-	4.0	6.8×10^{-2}
3^-	3^-	1.2	8.2×10^{-3}
5^-	3^-	0.4	8.5×10^{-1}
	$K^\pi=0_2^- \rightarrow K^\pi=0_2^-$		
3^-	1^-	38.8	0.21
5^-	3^-	36.5	0.18

TABLE VII. Coulomb shifts and energies in ^{22}Mg.

J^π	$\Delta E_{\rm GCM}$	$E_x^{\rm predicted}$	$E_x^{\rm exp}$
	$K^\pi=0_1^+$		
0^+	1.25	0	0
2^+	1.25	1.27	1.25
4^+	1.22	3.33	3.31
6^+	1.26	6.32	
8^+	1.37	11.12	
	$K^\pi=2^+$		
2^+	1.14	4.35	4.40
3^+	1.17	5.56	
4^+	1.24	6.34	6.22
5^+	1.22	9.58	
	$K^\pi=1^+$		
1^+	1.24	5.34	5.32
2^+	1.25	5.36	5.29
3^+	1.21	7.27	
4^+	1.24	5.51	5.46
5^+	1.21	7.37	
	$K^\pi=1^-$		
1^-	1.11	6.91	
2^-	1.05	7.46	
3^-	1.05	7.52	
4^-	1.04	8.26	
5^-	1.06	10.42	

the experiment of Alford *et al.*[9] The Coulomb shifts obtained for negative-parity states are somewhat smaller than in positive parity. We suggest a 1^- band whose head is located near 6.9 MeV.

Let us come back to the full GCM approach. In Table VIII, we present the theoretical $B(E2)$ between low-lying ^{22}Mg states. In the ground-state band, the $B(E2)$ values are larger than in the analog band of ^{22}Ne. This suggests a more important clustering in the 0_1^+ band of ^{22}Mg than of ^{22}Ne.

V. THE ^{18}O$(\alpha,\gamma)^{22}$Ne CAPTURE REACTION

The ^{18}O$(\alpha,\gamma)^{22}$Ne capture reaction plays an important role in astrophysical applications since it is one of the basic reactions from which heavier elements can be produced.[10] The capture cross section has been experimentally investigated by Adams *et al.*[23] in the energy range $E_\alpha=2.15-3.70$ MeV. Since the energies of astrophysical interest are significantly lower, Trautvetter *et al.*[10] have studied the ^{22}Ne spectrum near the $\alpha+^{18}$O threshold, and deduced the $\omega\gamma$ values of the relevant resonances. However, the direct contribution was determined in a very simple theoretical model. Since the direct-capture process strongly affects the reaction rate at low temperatures ($T_9\lesssim0.1$, from Ref. 10), it is worthwhile to reanalyze it in the present microscopic framework.

Let us first discuss the results at energies close to the Coulomb barrier. The data of Adams *et al.*[23] are compared with the GCM calculation in Fig. 5. The final states involved in the calculation are the 0^+ (g.s.), 2^+ (1.27 MeV), 2^+ (4.46 MeV), 0^+ (6.24 MeV), 1^- (7.05 MeV), and 1^- (7.49 MeV) states. The capture cross section in this energy range mainly arises from the $1^-\rightarrow0^+$ (g.s.) and $1^-\rightarrow2^+$ (1.27 MeV) $E1$ transitions. At the lowest energies, the theory agrees with experiment. The experimental data are consistent with a resonance near 1.8 MeV due, in our calculation, to the 1^- ($E_{\rm c.m.}=1.8$ MeV) resonance. Beyond 2 MeV, the GCM underestimates the data. Most likely, the experimental points are affected by many resonances which are missing in the model. Near 2.2 and 2.8 MeV, the sharp bumps in the GCM curve correspond to the 2^+ and 3^- resonances, respectively (see Sec. IV B). Let us now turn to the capture reaction at low energies. The $E1$ and $E2$ S factors labeled by the final states are displayed in Fig. 6. Both components present sharp resonances at 0.61 MeV (0^+), 0.65 MeV (3^-), 1.25 MeV (2^+), and 1.80 MeV (1^-). Below 0.5 MeV, the S factor is dominated by the contribution of the 0^+ resonance, which is expected to determine the re-

TABLE VIII. Theoretical $E2$ reduced transition probabilities (in W.u.) in ^{22}Mg.

$J_i^{\pi_i}$	$J_f^{\pi_f}$	$B(E2)$
	$K^\pi=0_1^+ \rightarrow K^\pi=0_1^+$	
2^+	0^+	13.3
4^+	2^+	17.7
6^+	4^+	12.9
8^+	6^+	7.3
	$K^\pi=2^+ \rightarrow K^\pi=2^+$	
2^+	0^+	1.6
	2^+	3.4
	4^+	2.3×10^{-3}
3^+	2^+	2.2
	4^+	0.3

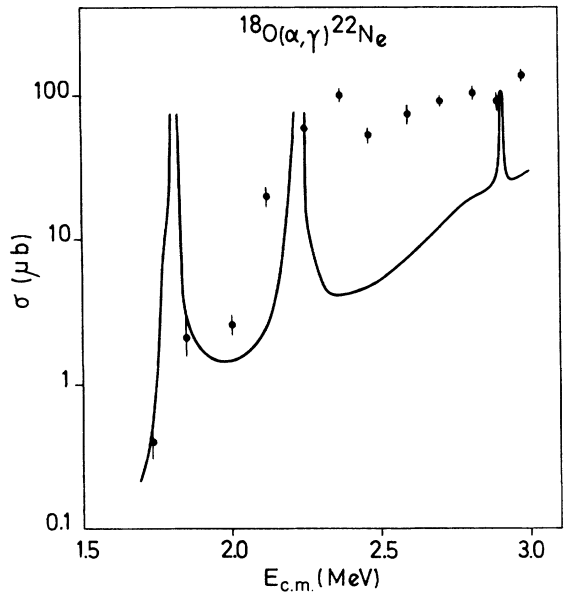

FIG. 5. $^{18}O(\alpha,\gamma)^{22}Ne$ capture cross section as a function of the c.m. energy. The experimental data are from Ref. 23.

action rate at low temperatures. Trautvetter *et al.*[10] have observed a state at $E_{c.m.}=0.54$ MeV, i.e., below the 0^+ resonance, but the spin is uncertain. However, this state is certainly not a 0^+ state,[10] and hence it is not expected to affect the S factor at stellar energies. Our calculation does not support the existence of other states in the vicinity of the $\alpha+^{18}O$ threshold. With the present S factor, the reaction rate can be determined by numerical integration of the cross section times a Maxwell-Boltzmann distribution. The reaction rate is divided in a direct capture and resonant terms. The direct-capture contribution, essentially due to the 0^+ partial wave can be parametrized by

$$\langle \sigma v \rangle = 1.18\times 10^3 (1-4.9T_9^{1/3}+12.1T_9^{2/3})T_9^{-2/3} \times \exp(-40.04T_9^{-1/3}) \ . \quad (20)$$

This term represents the dominant contribution to the reaction rate for temperatures lower than 10^8 K. In this range the present reaction rate is about five times larger than the reaction rate recommended in astrophysical applications.[11] For this comparison, we use the lower limit of Ref. 11, which is based on the assumption (supported by our theoretical study) that no additional state exists in the vicinity of the $\alpha+^{18}O$ threshold.

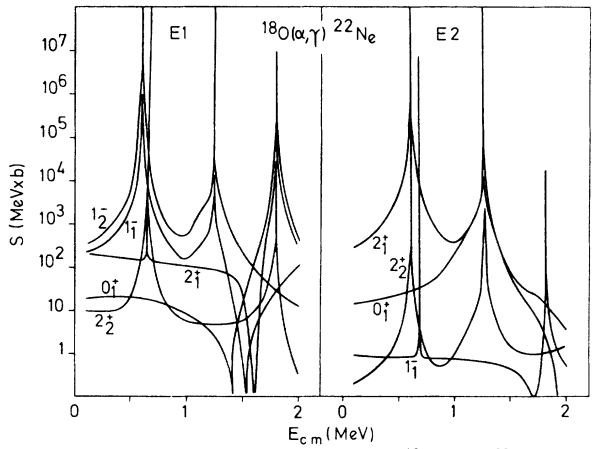

FIG. 6. $E1$ and $E2$ components of the $^{18}O(\alpha,\gamma)^{22}Ne$ S factor. The curves are labeled by the corresponding ^{22}Ne final states.

For temperatures higher than 10^8 K, the reaction rate is given by the contribution of low-lying resonances. The resonant reaction rate is completely defined by the location of the resonances,and their strengths $\omega\gamma$. Although several low-lying resonances are present in the model, some relevant resonances, such as the lowest one at $E_x=10.20$ MeV, are missing. The structure of the missing resonances is probably different from the $\alpha+^{18}O(0^+,2^+)$ structure adopted here. Therefore, a valuable theoretical description of the $^{18}O(\alpha,\gamma)^{22}Ne$ resonant capture rate should require additional configurations.

VI. CONCLUSION

In this paper we have shown that the three-cluster model succeeds in reproducing many properties of the ^{22}Ne nucleus. We have suggested the existence of several bands, and have proposed experimental candidates. The model predicts a 0_3^+ band located around the Coulomb barrier and whose states present a marked $\alpha+^{18}O$ structure. It is interesting to point out that a similar band has been obtained in the $\alpha+^{20}Ne$ study[5] of ^{24}Mg. Without any effective charge, we reproduce fairly well the $B(E2)$ in the ^{22}Ne nucleus. We have also suggested spin assignments for different states in the ^{22}Mg mirror nucleus, based on the experimental energies of ^{22}Ne and on the GCM Coulomb shifts.

We have presented the $E1$ and $E2$ components of the $^{18}O(\alpha,\gamma)^{22}Ne$ capture cross section, which is dominated by several resonances. The most important one is the 0^+ (10.28 MeV) state which determines the S factor at stellar energies. We have proposed a parametrization of the GCM nonresonant reaction rate, which is larger by a factor of 5 than the recommendation of Caughlan *et al.*[11] Trautvetter *et al.*[10] have suggested that additional resonances could exist in the vicinity of the $\alpha+^{18}O$ threshold, and therefore the reaction rate could be significantly enhanced. The present study does not support this conjecture, and hence does not suggest any modification to the resonant reaction rate of Trautvetter *et al.*

The model could be improved by the introduction of the $n+^{21}Ne$ channel open 0.70 MeV only above the $\alpha+^{18}O$ threshold, or by describing the ^{18}O nucleus by an $\alpha+^{14}C$ structure. This description would allow one to introduce negative-parity states of ^{18}O and hence to reproduce different ^{22}Ne states missing in the present model. However, both improvements require a tremendous increase in the complexity of the calculation. The present description of the ^{22}Ne nucleus provides satisfactory results, and remains relatively simple in its principle.

ACKNOWLEDGMENTS

I am grateful to Dr. D. Baye for many helpful discussions and for his careful reading of my manuscript. This work was supported by the Fonds National de la Recherche Scientifique.

[1]Y. C. Tang, in *Topics in Nuclear Physics II,* Vol. 145 of *Lecture Notes in Physics* (Springer, Berlin, 1981), p. 572.
[2]D. Baye and P. Descouvemont, *Proceedings of the Workshop on Relation Between Structure and Reactions in Nuclear Physics, Drexel,* edited by D. H. Feng, M. Vallieres, and B. H. Wildenthal (World-Scientific, Singapore, 1986), p. 27.
[3]Y. Fujiwara, H. Horiuchi, K. Ikeda, M. Kamimura, K. Katō, Y. Suzuki, and E. Uegaki, Prog. Theor. Phys. Suppl. **68**, 29 (1980).
[4]P. Descouvemont and D. Baye, Phys. Rev. C **36**, 54 (1987).
[5]P. Descouvemont and D. Baye, Nucl. Phys. **A475**, 219 (1987).
[6]P. Descouvemont and D. Baye, Phys. Rev. C **31**, 2274 (1985).
[7]K. Langanke, Nucl. Phys. **A373**, 493 (1982).
[8]K. Langanke, D. Frekers, R. Stademann, and A. Weiguny, Nucl. Phys. **A402**, 40 (1983).
[9]W. P. Alford, P. Craig, D. A. Lind, R. S. Raymond, J. Ullman, C. D. Zafiratos, and B. H. Wildenthal, Nucl. Phys. **A457**, 317 (1986).
[10]H. P. Trautvetter, M. Wiescher, K.-U. Kettner, C. Rolfs, and J. W. Hammer, Nucl. Phys. **A297**, 489 (1978).
[11]G. R. Caughlan, W. A. Fowler, M. J. Harris, and B. A. Zimmerman, At. Data Nucl. Data Tables **32**, 197 (1985).
[12]F. Ajzenberg-Selove, Nucl. Phys. **A375**, 1 (1982).
[13]D. Baye and P. Descouvemont, Nucl. Phys. **A419**, 397 (1984).
[14]P. Descouvemont, Nucl. Phys. **A470**, 309 (1987).
[15]D. Baye, P.-H. Heenen, and M. Libert-Heinemann, Nucl. Phys. **A308**, 229 (1978).
[16]D. Baye and P. Descouvemont, Nucl. Phys. **A407**, 77 (1983).
[17]P. M. Endt and C. van der Leun, Nucl. Phys. **A310**, 1 (1978).
[18]C. Broude, W. G. Davies, J. S. Forster, and G. C. Ball, Phys. Rev. C **13**, 953 (1976).
[19]E. M. Szanto, A. Szanto de Toledo, H. V. Klapdor, G. Rosner, and M. Schrader, Nucl. Phys. **A404**, 142 (1973).
[20]G. Chouraqui, T. Muller, M. Port, and J. M. Thirion, J. Phys. (Paris) **31**, 249 (1970).
[21]L. K. Fifield, R. W. Zurmuhle, D. P. Balamuth, and S. L. Tabor, Phys. Rev. C **13**, 1515 (1976).
[22]A. Bohr and B. R. Mottelson, *Nuclear Structure* (Benjamin, Massachusetts, 1975), Vol. 2.
[23]A. Adams, M. H. Shapiro, W. M. Denny, E. G. Adelberger, and C. A. Barnes, Nucl. Phys. **A131**, 430 (1969).